ACS APPLIED BIO MATERIALS



Article

# A Multilevel Nanoarchitecture Exhibiting Biosensing for Cancer Diagnostic by Dual Modal Switching of Optical and Magnetic Resonance Signals

Ruichan Lv, Miao Feng, Liyang Xiao, Jossana Damasco, Jie Tian, and Paras N. Prasad

*ACS Appl. Bio Mater.*, **Just Accepted Manuscript** • DOI: 10.1021/acsabm.8b00429 • Publication Date (Web): 18 Oct 2018



ACS Publications

is published by the American Chemical Society. 1155 Sixteenth Street N.W., Washington, DC 20036

# A Multilevel Nanoarchitecture Exhibiting Biosensing for Cancer Diagnostic by Dual Modal Switching of Optical and Magnetic Resonance Signals

*Ruichan Lv[a,b,*], Miao Feng[b], Liyang Xiao[b], Jossana A. Damasco[a], Jie Tian[b,*], Paras N. Prasad[a,*]*

a. Institute for Lasers, Photonics, and Biophotonics and Department of Chemistry, University at Buffalo, the State University of New York, Buffalo, NY 14260, USA

b. Engineering Research Center of Molecular and Neuro Imaging, Ministry of Education, School of Life Science and Technology, Xidian University, Xi'an, Shanxi 710071, China

*E-mail: rclv@xidian.edu.cn; jie.tian@ia.ac.cn; pnprasad@buffalo.edu

**ABSTRACT**

In this research, the fabrication and application of a multifunctional core-shell nanoarchitecture was proposed. $NaYF_4$:Yb,Er@$NaYF_4$:Yb,Nd exhibits upconversion luminescence (UCL) of Erbium ions, but has quenched UCL emission when coated with $MnO_2$ nanosheets. This hierarchical multilevel UCNP-$MnO_2$ exhibits restoration of UCL

and generation of magnetic resonance imaging (MRI) signal when exposed to the microenvironment containing glutathione (GSH)/$H_2O_2$, which strips the $MnO_2$ sheets by converting it to paramagnetic $Mn^{2+}$ ions. This dual-modal switching feature of the optical emission and MRI signals provides the platform as stimuli-responsive biosensing of GSH/$H_2O_2$. Our new formulation as a dual-modal biosensor for detecting aberrant levels of intracellular GSH/$H_2O_2$ associated in cancer cells could be a potential diagnostic probe to distinguish the tumor cells from normal cells.

**KEY WORDS:** Up-Conversion, MRI signal, Stimuli-Responsive, Biosensing.

## INTRODUCTION

Early detection of cancer cells is essential for the disease control and prevention. An ultrasensitive detection platform is challenging due to only small changes of cancer biomarkers in the early stage of disease. Molecular imaging is a powerful tool for early detection and treatment of disease in malignant tumors, especially for the diagnosis of micro tumor focus.[1-5] Dual-/multi-modal molecular imaging method can coordinate sensitivity, resolution and tissue penetration degree under the same condition to detect micro tumor focus.[6-8] For example, magnetic resonance imaging (MRI) with high spatial resolution and tissue penetrability but poor sensitivity could be combined with fluorescent imaging with limited tissue penetration but high sensitivity[9-10], and the combination of these imaging modalities can be of significant value for dual-/multi-modal imaging guided therapy or surgery.[11-14]

In mammalian cells, the glutathione (L-γ-glutamyl-L-cysteinyl-glycine, named as GSH) is the most abundant thiolated tripeptide. Generally, intracellular concentrations of GSH between 0.5 and 10 mM are typically observed, and extracellular GSH concentrations are considerably lower, with estimated values in the micromolar range. The level of GSH could be used for staging of cancer, aging, and heart problems.[15-19] In another part, higher amount of $H_2O_2$ generated when normal cells transferred to cancer cells, while more $H_2O_2$ could kill the cancer cells (this is the fundamental thought to the proposed photodynamic therapy). Without outside intervention, higher but not too much $H_2O_2$ exist in cancer cells. When much more $H_2O_2$ intervened into cancer cells,

the cells could be killed by reactive oxygen species. As known there is abnormal concentration level of these two GSH/ $H_2O_2$ biomarkers, yet it was hard to form a unified conclusion whether they were high or low in different cancer cell lines, no matter from qualitative part or quantitative part. However, the definite point is that the concentration levels of GSH and $H_2O_2$ are abnormal in the cancer cells compared with the normal cells. Thus, it was meaningful to find nanoprobes to detect them. Traditional bio-probes to monitor the GSH levels are thiol-sensitive organic dyes, which always use the ultra-violet light or visible light as the irradiation source.[20] The organic dyes could be sensitive to GSH levels, but they were not suitable for long-time detection because they were easy to photo-bleaching and the ultra-violet/ visible light had limited penetration in the cells and tissues.

Up-conversion nanoparticles (UCNPs) can convert deep tissue penetrating near-infrared (NIR) light to another shorter wavelength light has emerged as an important nanoprobe for optical imaging and sensing.[21-26] UCNPs have many advantaged features such as, high physical/chemical stability and photostability, improved signal-to-noise ratios without auto-fluorescence using NIR irradiation, and high tissue penetration depth of the incident NIR light. [27-39] Despite there were some literatures about combination of UCNPs with $MnO_2$ nanosheets as the quencher and reducer when detecting the cancer cells[40-45], there are still several challenges to be resolved: (I) The synthesis procedure is expected to be facile and simple with high yield, and the final morphology of the stimuli-responsive agent should be improved. (II) There is no literature to detect the GSH levels

using 808 nm as the irradiation laser, of which the 808 nm laser has higher penetration depth than that of 980 nm and much lower heating injury to the tissues and body. (III) Limited by the upconvertion efficiency, the detection sensitivity and accuracy were expected to be improved, and it was meaningful to find nanoprobes with adjustable detection ranges.

In this paper, we introduce a nanoformulation involving an upconversion nanoparticle with a core containing Erbium for upconversion luminescence under 808 nm laser, and then coated with $MnO_2$ nanosheets for biosensing of the level of GSH/$H_2O_2$ which could be used to distinguish cancer form normal cells. The design of our nanoconstruct is presented in **Scheme 1**. The nanoplatform of $NaYF_4$:Yb,Er@$NaYF_4$:Yb,Nd exhibits upconversion under 808 nm light by absorption in Nd, then energy transfer to Yb which sensitizes Er to emit upconverted light at 543 and 654 nm. The $MnO_2$ nano-sheets generated on the surface of UCNPs, serves as an efficient quencher for UCL without MRI signal. The luminescence intensity recovers and MR contrast generates by adding a small amount of GSH or $H_2O_2$ that strips off $MnO_2$ by reducing it to into $Mn^{2+}$. As known there is abnormal amount of GSH or $H_2O_2$ in tumor cells, thus UCNPs-$MnO_2$ serves as a sensitive probe for GSH and $H_2O_2$ in tumor cells.[16, 41, 46]

## EXPERIMENTAL

### Materials

All chemical reagents used are analytical grade without any further purification.

$Y(CH_3COO)_3$ (99.9%), $Er(CH_3COO)_3$ (99.9%), $Yb(CH_3COO)_3$ (99.9%), $Y_2O_3$ (99.99%), $Yb_2O_3$ (99.99%), $Nd_2O_3$ (99.99%),and sodium trifluoroacetate ($CF_3COONa$, 98%) were obtained from Sinopharm Chemical Reagent Co., Ltd., Shanghai, China. Oleic acid (OA, technical grade), oleylamine (OM), 1-octadecene (ODE, technical grade), trifluoroacetic acid ($CF_3COOH$, 99%), sublimed sulfur (S), polyethylenimine (MW = 25000), glycerol, were purchased from Sigma-Aldrich, China. Cyclohexane, phosphatebuffered saline (PBS), glutaraldehyde, and dimethyl sulfoxide (DMSO) were obtained from Tianjin Kermel Chemical Reagent Co., Ltd., Tianjin, China.

**Synthesis of $NaYF_4$:18%Yb,2%Er@ $NaYF_4$:30%Yb,10%Nd.**

In a typical procedure, the core of $NaYF_4$:18%Yb,2%Er and the core@shell of $NaYF_4$:18%Yb,2%Er@$NaYF_4$:30%Yb,10%Nd (noted as UCNPs) were firstly synthesized according to our published literature.[47] The as-synthesized hydrophobic UCNPs precipitate was dispersed in hexane for further use.

**Synthesis of hydrophilic UCNPs-S**

The hydrophobic UCNPs were coated with a sulfide (S) shell following a reported procedure[48]. Typically, 1 mmol of sulfide powder was dissolved in 3 mL of oleylamine (OM) and sonicated for 5 min to obtain a brown solution. The solution is then put into a three-necked flask together with 1 mmol UCNPs in 10 mL of hexane. The flask was then heated and kept at 70 °C for 40 min before it was allowed to cool to room temperature. The solution was subsequently washed and centrifuged with ethanol to collect the yellow

UCNPs-S precipitate. To prepare the hydrophilic UCNPs-S, 0.2 mmol of UCNPs-S was mixed with CTAB (0.1 g in 20 mL of deionized water) and stirred for 12 h. The hydrophilic UCNPs-S was obtained after twice washing and centrifugation with deionized water.

**Synthesis of UCNPs-$MnO_2$**

The hydrophilic UCNPs-S (1 mM) was dispersed in 5 mL of water before adding 1 mL of aqueous $KMnO_4$ solution (0.15 mg/mL) drop by drop and stirring for 2 h at room temperature. A change in the color of solution from purple to brown was observed indicating the reduction of $KMnO_4$ to $MnO_2$ by the sulfides on the UCNPs-S surface. Water was then added to the brown solution and then centrifuged. This procedure was repeated three times before collecting the brown UCNPs-$MnO_2$ precipitate.

**Characterization**

The morphologies were detected by transmission electron microscopy (TEM, FEI Tecnai $G^2$ S-Twin). Dynamic light scattering (DLS) analysis of the materials is detected by ZEN3690 (Malvern). UCL spectra were obtained on a spectrofluorometer (FLS 950) using 808 nm laser diode Module (MDL-III-808-2.5W). The ultraviolet visible (UV-vis) absorbance spectra were measured by a UV-1601 spectrophotometer.

***In Vitro* Viability of UCNPs-$MnO_2$.**

Typically, MCF-7 cells were incubated in the 96-well plate (6000-7000 cells per well). After the monolayer cells obtained, UCNPs-$MnO_2$ with concentrations of 500, 250, 125, 62.5, 31.3, 15.63, and 7.81 μg/mL were added in 7 groups with at least 3 wells in each

group. The control group without any materials added was regarded as the 100% growth. After further incubated for 24 h, 20 μL of MTT solution (5 mg/mL) was added into each well and incubated for another 4 h. Finally, the culture in the plate was discarded and 150 μL of DMSO was added into each well. The absorbance at 490 nm of the solution in each well was recorded by a micro-plate reader.

In another 6-well plate, the cells were incubated with the UCNPs-$MnO_2$ (1 mg/mL) together with coverslip for 24 h, and then the cells were rinsed with PBS. The coverslip was put onto the glass slide for final use. The optical microscopy images of cells incubated with UCNPs-$MnO_2$ was taken by optical microscope.

**RESULTS AND DISCUSSION**

TEM images of the core $NaYF_4$:Yb,Er and core/shell NaYF4:Yb,Er@ $NaYF_4$:Yb,Nd UCNPs in **Figure 1**A and 1B indicate that the synthesized nanocrystals are uniform with average sizes of 25 nm and 32 nm, respectively. Uniform UCNPs are essential for further sulfide coating. When enhanced amounts of $KMnO_4$ were added, $MnO_2$ nanosheet increased accordingly. Figure 1C shows the formation of thin $MnO_2$ nanosheets due to the reduction of $KMnO_4$ by the sulfide. In this study, formation of the $MnO_2$ nanosheets on the surface of the UCNPs-S was directed by its sulfide coating. TEM images of UCNPs-$MnO_2$ with different amount of $KMnO_4$ added to the sulfide coated NP are presented in Figure 1D-F. As expected, increased amount of $KMnO_4$ from 1 mg to 3 mg could react with the sulfide coating on the UCNPs, which result in the formation of more and thicker $MnO_2$ nanosheets. However, increasing the amount of $KMnO_4$ to 3 mg results in the self-assembly

of $MnO_2$ nanosheets, instead of forming on the surface of UCNPs. We have also utilized another synthesis strategy according to our previous successful experience.[47] In this method, UCNPs were first coated with 2 mL of polyacrylic acid (concentration: 0.5 g/mL) before reacting with the same amount of $KMnO_4$. TEM images of the generated compound is shown in **Figure S1**, of which the structure on the surface of UCNPs is not $MnO_2$ nanosheet but block-shaped $MnO_2$.

Trace amount of GSH was added at a 10000: 6 molar ratio of UCNPs-$MnO_2$ to GSH under room temperature to test the sensitivity of UCNPs-$MnO_2$ to GSH. Upon addition of GSH, the $MnO_2$ nanosheets degrade as clearly shown in **Figure 2**, wherein the UCNPs were exposed, revealing almost complete reduction of the $MnO_2$ anosheet surface coating. Dynamic light scattering (DLS) from UCNPs-$MnO_2$ before and after $MnO_2$ reduction by GSH were measured as a function of number (**Figure S2**) and intensity (**Figure S3**). DLS results of the UCNPs-$MnO_2$ prior to reduction show good uniformity, with an average size of 130 nm (by number, PdI: 0.081) and 165 nm (by intensity, PdI: 0.133). Upon reduction by GSH, the DLS results showed 2 maxima at [226 nm and 164 nm] (by number, PdI: 0.094) and [149 nm and 947 nm] (by intensity, PdI: 0.256), which might be attributed to the disassembly of UCNPs-$MnO_2$ into two parts of UCNPs and other hydrophobic parts (white precipitate), with the hydrophobic parts rearranging into large aggregating form.[49-50]

The use of UCNPs-$MnO_2$ as a diagnostic probe for GSH sensing was confirmed by investigating the recovery of the upconversion luminescence upon addition of GSH. As

shown in **Figure 3,** the UCL intensity increases with increasing amount of added GSH. The $MnO_2$ nanosheet can quench UCL because there is florescence resonance energy transfer (FRET) effect between UCNPs and $MnO_2$ nanosheet. The maximum enhancement factors of different UCNPs-$MnO_2$ with increasing $MnO_2$ nanosheet thickness (corresponding to Figure 1B,D,F) versus the added amount of GSH, measured at the two Er emission wavelengths are 1.69, 2.26, 2.55 (543 nm), and 1.07, 1.69, 2.01 (654 nm), respectively. It can be observed that the highest enhancement factors for both wavelengths are from the nanoparticles with the thickest $MnO_2$ coating. Note that there is almost no change in the downconversion spectra in the NIR region (900 nm-1700 nm) with the addition of different amounts of GSH under 808 nm laser excitation, indicating that the quenching effect of $MnO_2$ did not occur in this region (**Figure S4**). It is interesting that the intensity of green upconverion emission (500-600 nm) has a higher enhancement factor than that of red upconversion emission (600-700 nm) and NIR emission (longer than 800 nm). The different effect on green, red, and NIR emission region because the absorbance intensities are different. As shown in **Figure S5**, there is higher absorbance in the shorter wavelength region of the UCNPs-$MnO_2$ solution. When there is no $MnO_2$ but only $Mn^{2+}$ ions in the UCNPs solution, the absorbance of UCNPs+$Mn^{2+}$ at the UV-vis region almost disappeared, resulting in disappeared quenching effect in these regions.

As shown in **Figure 4**A above, the color of UCNPs-$MnO_2$ solution changed from brown to colorless due to the reduction of $MnO_2$ to the $Mn^{2+}$ ions. Enhancement of the emitted light under NIR irradiation is observed because of the decreased absorbance in the

visible regions of the UCNPs-$MnO_2$ solution with the increasing amount of GSH (Figure 4B and **Figure S6**). The emitted lights of the UCNPs-$MnO_2$ with adjusted $H_2O_2$ added are also shown in **Figure S7**. This result is similar to that of GSH, indicating this platform could be responsive to $H_2O_2$ simultaneously. A series of electrolytes and biomolecules was chosen to test the selectivity of the UCNP-$MnO_2$ nanoparticles to GSH/$H_2O_2$. Typically, UCNP-$MnO_2$, the electrolytes ($H_2O_2$, NaCl, and NaOH), and biomolecules (GSH, glucose, PBS powder, serum, and medium) were dissolved into deionized water (Group 1 in **Figure S8**). Then, the electrolytes and biomolecules solutions were separately mixed with UCNPs-$MnO_2$ (Group 2 in Figure S8). After shaking for several seconds by hand, only the GSH/$H_2O_2$ recovered to the original colorless solution, and the reacted powders kept brown/black in other solutions (Group 3 in Figure S8). The absorbance intensity response of UCNPs-$MnO_2$ in different electrolytes and biomolecules solutions were shown in **Figure S9**, indicating there is obvious decrease of the absorbance in the GSH and $H_2O_2$ groups. That means, the UCNPs-$MnO_2$ have high selectivity to GSH/$H_2O_2$.

As is known, $MnO_2$ is reduced to the $Mn^{2+}$ ions in the presence of glutathione (GSH) or $H_2O_2$, resulting in the enhancement of the $T_1$ and $T_2$ relaxivity. MRI signal enhancement of the UCNPs-$MnO_2$ solution with the addition of GSH are shown in **Figure 5**. Both the T1 and T2 relaxation rates in water were measured at 1.5T to show that the UCNPs-$MnO_2$ could be used as MR contrast agent. Initially, the hybrid UCNPs-$MnO_2$ have relaxivity values of r1 = 1.23±0.06 $mM^{-1}$ $s^{-1}$ and r2 =15.0±0.66 $mM^{-1}$ $s^{-1}$. Upon addition of GSH, the quenched signal increased to r1 =2.71±0.11 $mM^{-1}$ $s^{-1}$ and r2 = 26.8±3.67 $mM^{-1}$ $s^{-1}$. This

two-fold increase in the MRI signals (r1: 2.20, r2: 1.79) clearly demonstrates the ability to utilize the UCNPs-$MnO_2$ to monitor GSH, which serve as "switch" to TURN ON the high MRI contrast.

The MCF-7 cells incubated with UCNPs-$MnO_2$ of different concentrations was carried out and the results are shown in **Figure 6**A. The viability values with different concentrations are high (93.6%-107.0%), indicating the good biocompatibility of this material. Meanwhile, the optical microscopy images of cells incubated with UCNPs-$MnO_2$ (concentration: 1 mg $mL^{-1}$) for 24 h was shown in Figure 6B, and the morphology of cells kept normal, revealing there is no side effect of UCNPs-$MnO_2$. This unique biosensing of GSH by "switching" ON the high MRI contrast, and the recovery of UCL together with its good biocompatibility make our material very promising bimodal diagnostic probe with very high potential for clinical translation.

## CONCLUSION

In summary, we have developed a switchable contrast agent, consist of optically active lanthanide UCNPs core and pre-magnetic $MnO_2$ nanosheet surface that can provide UCL and MR turning on imaging modalities simultaneously. The changes of UCL and MRI signal with added biomarkers could be used for intracellular diagnosis based on the amount of GSH or $H_2O_2$, which could be used to distinguish the cancer cells from normal cells. Thus, this UCNPs-$MnO_2$ platform would be a potential diagnostic probe for future clinical application.

## ASSOCIATED CONTENT

TEM images of UCNPs-$MnO_2$ with PAA modified on the UCNPs firstly. DLS results of UCNPs-$MnO_2$ before and after GSH reduced by number and intensity, respectively. Down-shifting spectra of different wavelengths of 900-1100 nm and 1200-1700 nm of UCNPs-$MnO_2$ with different amount of GSH added under 808 nm laser excitation. UV-vis absorbance spectra of UCNPs, UCNPs-$MnO_2$, and UCNPs+$Mn^{2+}$. The absorbance at 400 nm of UCNPs-$MnO_2$ versus the concentration of added GSH. Photographs of the UCNPs-$MnO_2$ solutions under ambient light and under 808 nm irradiation with different $H_2O_2$ added. Photographs of different electrolytes and biomolecules solutions response to UCNP-$MnO_2$. Absorbance change of different electrolytes and biomolecules solutions response to UCNP-$MnO_2$. This material is available free of charge via the Internet at http://pubs.acs.org.

## AUTHOR INFORMATION

### Corresponding Author

*E-mail: rclv@xidian.edu.cn; jie.tian@ia.ac.cn; pnprasad@buffalo.edu

### Author Contributions

The manuscript was written through contributions of all authors. All authors have given approval to the final version of the manuscript.

## ACKNOWLEDGMENT

Financial supports from the Fundamental Research Funds for the Central Universities, the

Natural Science Foundation of China (NSFC 81227901 and 81801744), and the National Key R&D Program of China Grant under No. 2017YFA0205200 are greatly acknowledged. At Buffalo, the research was supported by a grant (FA9550-15-1-0358) from the Air Force Office of Scientific Research.

## REFERENCES

(1) Gai, S.; Li, C.; Yang, P.; Lin, J., Recent Progress in Rare Earth Micro/Nanocrystals: Soft Chemical Synthesis, Luminescent Properties, and Biomedical Applications. *Chem. Rev.* **2013,** 114, 2343-2389.

(2) Antaris, A. L.; Chen, H.; Cheng, K.; Sun, Y.; Hong, G.; Qu, C.; Diao, S.; Deng, Z.; Hu, X.; Zhang, B.; Zhang, X.; Yaghi, O. K.; Alamparambil, Z. R.; Hong, X.; Cheng, Z.; Dai, H., A Small-Molecule Dye for NIR-II Imaging. *Nat. Mater.* **2016,** 15, 235-243.

(3) Yang, Z. G.; Sharma, A.; Qi, J.; Peng, X.; Lee, D. Y.; Hu, R.; Lin, D. Y.; Qu, J. L.; Kim, J. S., Super-Resolution Fluorescent Materials: an Insight into Design and Bioimaging Applications. *Chem. Soc. Rev.* **2016,** 45, 4651-4667.

(4) Jiang, K.; Sun, S.; Zhang, L.; Lu, Y.; Wu, A.; Cai, C.; Lin, H., Red, Green, and Blue Luminescence by Carbon Dots: Full-Color Emission Tuning and Multicolor Cellular Imaging. *Angew. Chem. Int. Ed.* **2015,** 54, 5360-5363.

(5) Ai, X.; Ho, C. J. H.; Aw, J.; Attia, A. B. E.; Mu, J.; Wang, Y.; Wang, X.; Wang, Y.; Liu, X.; Chen, H.; Gao, M.; Chen, X.; Yeow, E. K. L.; Liu, G.; Olivo, M.; Xing, B., In Vivo Covalent Cross-Linking of Photon-Converted Rare-Earth Nanostructures for Tumour Localization and Theranostics. *Nature Comm.* **2016,** 7, 10432.

(6) Gnach, A.; Lipinski, T.; Bednarkiewicz, A.; Rybka, J.; Capobianco, J. A., Upconverting Nanoparticles: Assessing the Toxicity. *Chem. Soc. Rev.* **2015,** 44, 1561-1584.

(7) Wolfbeis, O. S., An Overview of Nanoparticles Commonly Used in Fluorescent Bioimaging. *Chem. Soc. Rev.* **2015,** 44, 4743-4768.

(8) Nie, L. M.; Chen, X. Y., Structural and Functional Photoacoustic Molecular

Tomography Aided by Emerging Contrast Agents. *Chem. Soc. Rev.* **2014,** 43, 7132-7170.

(9) Na, H. B.; Song, I. C.; Hyeon, T., Inorganic Nanoparticles for MRI Contrast Agents. *Adv. Mater.* **2009,** 21, 2133-2148.

(10) Verma, K. D.; Massing, J. O.; Kamper, S. G.; Carney, C. E.; MacRenaris, K.; Basilion, J. P.; Meade, T. J., Synthesis and Evaluation of MR Probes for Targeted-Reporter Imaging. *Chem. Sci.* **2017,** 8, 5764-5768.

(11) Lu, W.; Arumugam, R.; Senapati, D.; Singh, A. K.; Arbneshi, T.; Khan, S. A.; Yu, H.; Ray, P. C., Multifunctional Oval-Shaped Gold-Nanoparticle-Based Selective Detection of Breast Cancer Cells Using Simple Colorimetric and Highly Sensitive Two-Photon Scattering Assay. *ACS Nano* **2010,** 4, 1739-1749.

(12) Sun, Y.; Ding, M.; Zeng, X.; Xiao, Y.; Wu, H.; Zhou, H.; Ding, B.; Qu, C.; Hou, W.; Er-bu, A. G. A.; Zhang, Y.; Cheng, Z.; Hong, X., Novel Bright-Emission Small-Molecule NIR-II Fluorophores for in Vivo Tumor Imaging and Image-Guided Surgery. *Chem. Sci.* **2017,** 8, 3489-3493.

(13) Yang, Y.; Lin, L.; Jing, L.; Yue, X.; Dai, Z., CuInS2/ZnS Quantum Dots Conjugating Gd(III) Chelates for Near-Infrared Fluorescence and Magnetic Resonance Bimodal Imaging. *ACS Appl. Mater. Inter.* **2017,** 9, 23450-23457.

(14) Yang, T.; Tang, Y. a.; Liu, L.; Lv, X.; Wang, Q.; Ke, H.; Deng, Y.; Yang, H.; Yang, X.; Liu, G.; Zhao, Y.; Chen, H., Size-Dependent $Ag_2S$ Nanodots for Second Near-Infrared Fluorescence/Photoacoustics Imaging and Simultaneous Photothermal Therapy. *ACS Nano* **2017,** 11, 1848-1857.

(15) Yang, L.; Gao, M. X.; Zhan, L.; Gong, M.; Zhen, S. J.; Huang, C. Z., An enzyme-induced Au@Ag Core-Shell Nanostructure Used for an Ultrasensitive Surface-Enhanced Raman Scattering Immunoassay of Cancer Biomarkers. *Nanoscale* **2017,** 9, 2640-2645.

(16) Fan, W.; Bu, W.; Shen, B.; He, Q.; Cui, Z.; Liu, Y.; Zheng, X.; Zhao, K.; Shi, J.,

Intelligent $MnO_2$ Nanosheets Anchored with Upconversion Nanoprobes for Concurrent pH-/$H_2O_2$-Responsive UCL Imaging and Oxygen-Elevated Synergetic Therapy. *Adv. Mater.* **2015,** 27, 4155-4161.

(17) Han, H. S.; Choi, K. Y.; Lee, H.; Lee, M.; An, J. Y.; Shin, S.; Kwon, S.; Lee, D. S.; Park, J. H., Gold-Nanoclustered Hyaluronan Nano-Assemblies for Photothermally Maneuvered Photodynamic Tumor Ablation. *ACS Nano* **2016,** 10, 10858-10868.

(18) He, Y. Y.; Zhou, J.; Ma, S. N.; Nie, Y.; Yue, D.; Jiang, Q.; Wali, A. R. M.; Tang, J. Z.; Gu, Z. W., Multi-Responsive "Turn-On" Nanocarriers for Efficient Site-Specific Gene Delivery In Vitro and In Vivo. *Adv. Healthc. Mater.* **2016,** 5, 2799-2812.

(19) Ju, E.; Dong, K.; Chen, Z.; Liu, Z.; Liu, C.; Huang, Y.; Wang, Z.; Pu, F.; Ren, J.; Qu, X., Copper(II)-Graphitic Carbon Nitride Triggered Synergy: Improved ROS Generation and Reduced Glutathione Levels for Enhanced Photodynamic Therapy. *Angew. Chem. Int. Ed.* **2016,** 55, 11467-11471.

(20) He, D.; He, X.; Wang, K.; Yang, X.; Yang, X.; Zou, Z.; Li, X., Redox-Responsive Degradable Honeycomb Manganese Oxide Nanostructures as Effective Nanocarriers for Intracellular Glutathione-Triggered Drug Release. *Chem. Commun.* **2015,** 51, 776-779.

(21) Mai, H.-X.; Zhang, Y.-W.; Sun, L.-D.; Yan, C.-H., Highly Efficient Multicolor Up-Conversion Emissions and Their Mechanisms of Monodisperse $NaYF_4$:Yb,Er Core and Core/Shell-Structured Nanocrystals. *J. Phys. Chem. C* **2007,** 111, 13721-13729.

(22) Wang, Y.; Song, S.; Liu, J.; Liu, D.; Zhang, H., ZnO-Functionalized Upconverting Nanotheranostic Agent: Multi-Modality Imaging-Guided Chemotherapy with On-Demand Drug Release Triggered by pH. *Angew. Chem. Int. Ed.* **2015,** 54, 536-540.

(23) Li, R.; Ji, Z.; Dong, J.; Chang, C. H.; Wang, X.; Sun, B.; Wang, M.; Liao, Y.-P.; Zink, J. I.; Nel, A. E.; Xia, T., Enhancing the Imaging and Biosafety of Upconversion Nanoparticles through Phosphonate Coating. *ACS Nano* **2015,** 9, 3293-3306.

(24) Min, Y.; Li, J.; Liu, F.; Yeow, E. K. L.; Xing, B., Near-Infrared Light-Mediated

Photoactivation of a Platinum Antitumor Prodrug and Simultaneous Cellular Apoptosis Imaging by Upconversion-Luminescent Nanoparticles. *Angew. Chem. Int. Ed.* **2014,** 53, 1012-1016.

(25) Ai, X.; Lyu, L.; Zhang, Y.; Tang, Y.; Mu, J.; Liu, F.; Zhou, Y.; Zuo, Z.; Liu, G.; Xing, B., Remote Regulation of Membrane Channel Activity by Site-Specific Localization of Lanthanide-Doped Upconversion Nanocrystals. *Angew. Chem. Int. Ed.* **2017,** 56, 3031-3035.

(26) Das, G. K.; Tan, T. T. Y., Rare-Earth-Doped and Codoped $Y_2O_3$ Nanomaterials as Potential Bioimaging Probes. *J. Phys. Chem. C* **2008,** 112, 11211-11217.

(27) Yue, X.; Zhang, Q.; Dai, Z., Near-Infrared Light-Activatable Polymeric Nanoformulations for Combined Therapy and Imaging of Cancer. *Adv. Drug Deliver. Rev.***2017,** 115, 155-170.

(28) Lin, H.; Yu, T.; Tsang, M.-K.; Bai, G.; Zhang, Q.; Hao, J., Near-Infrared-to-Near-Infrared Down-Shifting and Upconversion Luminescence of $KY_3F_{10}$ with Single Dopant of $Nd^{3+}$ Ion. *Appl. Phys. Lett.* **2016,** 108, 041902.

(29) Liu, K.; Liu, X.; Zeng, Q.; Zhang, Y.; Tu, L.; Liu, T.; Kong, X.; Wang, Y.; Cao, F.; Lambrechts, S. A. G.; Aalders, M. C. G.; Zhang, H., Covalently Assembled NIR Nanoplatform for Simultaneous Fluorescence Imaging and Photodynamic Therapy of Cancer Cells. *ACS Nano* **2012,** 6, 4054-4062.

(30) Yang, Y.; Liu, J.; Sun, X.; Feng, L.; Zhu, W.; Liu, Z.; Chen, M., Near-Infrared Light-Activated Cancer Cell Targeting and Drug Delivery with Aptamer-Modified Nanostructures. *Nano Res.* **2016,** 9, 139-148.

(31) Chen, G.; Roy, I.; Yang, C.; Prasad, P. N., Nanochemistry and Nanomedicine for Nanoparticle-Based Diagnostics and Therapy. *Chem. Rev.* **2016,** 116, 2826-2885.

(32) Carlos, L. D.; Ferreira, R. A. S.; Bermudez, V. d. Z.; Julian-Lopez, B.; Escribano, P., Progress on Lanthanide-Based Organic-Inorganic Hybrid Phosphors. *Chem. Soc. Rev.* **2011,** 40, 536-549.

(33) Zheng, W.; Huang, P.; Tu, D.; Ma, E.; Zhu, H.; Chen, X., Lanthanide-Doped Upconversion Nano-Bioprobes: Electronic Structures, Optical Properties, and Biodetection. *Chem. Soc. Rev.* **2015,** 44, 1379-1415.

(34) Gorris, H. H.; Wolfbeis, O. S., Photon-Upconverting Nanoparticles for Optical Encoding and Multiplexing of Cells, Biomolecules, and Microspheres. *Angew. Chem. Int. Ed.* **2013,** 52, 3584-3600.

(35) Zhao, J.; Jin, D.; Schartner, E. P.; Lu, Y.; Liu, Y.; Zvyagin, A. V.; Zhang, L.; Dawes, J. M.; Xi, P.; Piper, J. A.; Goldys, E. M.; Monro, T. M., Single-Nanocrystal Sensitivity Achieved by Enhanced Upconversion Luminescence. *Nature Nanotech.* **2013,** 8, 729-734.

(36) Zhu, X.; Feng, W.; Chang, J.; Tan, Y.-W.; Li, J.; Chen, M.; Sun, Y.; Li, F., Temperature-Feedback Upconversion Nanocomposite for Accurate Photothermal Therapy at Facile Temperature. *Nature Comm.* **2016,** 7, 10437.

(37) Peng, J.; Xu, W.; Teoh, C. L.; Han, S.; Kim, B.; Samanta, A.; Er, J. C.; Wang, L.; Yuan, L.; Liu, X.; Chang, Y.-T., High-Efficiency in Vitro and in Vivo Detection of $Zn^{2+}$ by Dye-Assembled Upconversion Nanoparticles. *J. Am. Chem. Soc.* **2015,** 137, 2336-2342.

(38) Escudero, A.; Becerro, A. I.; Carrillo-Carrion, C.; Nunez, N. O.; Zyuzin, M. V.; Laguna, M.; Gonzalez-Mancebo, D.; Ocana, M.; Parak, W. J., Rare Earth Based Nanostructured Materials: Synthesis, Functionalization, Properties and Bioimaging and Biosensing Applications. *Nanophotonics* **2017,** 6, 881-921.

(39) Gargas, D. J.; Chan, E. M.; Ostrowski, A. D.; Aloni, S.; Altoe, M. V. P.; Barnard, E. S.; Sanii, B.; Urban, J. J.; Milliron, D. J.; Cohen, B. E.; Schuck, P. J., Engineering Bright Sub-10-nm Upconverting Nanocrystals for Single-Molecule Imaging. *Nature Nanotech.* **2014,** 9, 300-305.

(40) Deng, R.; Xie, X.; Vendrell, M.; Chang, Y.-T.; Liu, X., Intracellular Glutathione Detection Using $MnO_2$-Nanosheet-Modified Upconversion Nanoparticles. *J. Am.*

*Chem. Soc.* **2011,** 133, 20168-20171.

(41) Chen, Q.; Feng, L.; Liu, J.; Zhu, W.; Dong, Z.; Wu, Y.; Liu, Z., Intelligent Albumin-$MnO_2$ Nanoparticles as pH-/$H_2O_2$-Responsive Dissociable Nanocarriers to Modulate Tumor Hypoxia for Effective Combination Therapy. *Adv. Mater.* **2016,** 28, 7129-7136.

(42) Chen, X.; Wang, Y.; Chai, R.; Xu, Y.; Li, H.; Liu, B., Luminescent Lanthanide-Based Organic/Inorganic Hybrid Materials for Discrimination of Glutathione in Solution and within Hydrogels. *ACS Appl. Mater. Inter.* **2017,** 9, 13554-13563.

(43) Wang, Y.-F.; Liu, G.-Y.; Sun, L.-D.; Xiao, J.-W.; Zhou, J.-C.; Yan, C.-H., $Nd^{3+}$-Sensitized Upconversion Nanophosphors: Efficient In Vivo Bioimaging Probes with Minimized Heating Effect. *ACS Nano* **2013,** 7, 7200-7206.

(44) Xie, X.; Gao, N.; Deng, R.; Sun, Q.; Xu, Q.-H.; Liu, X., Mechanistic Investigation of Photon Upconversion in $Nd^{3+}$-Sensitized Core-Shell Nanoparticles. *J. Am. Chem. Soc.* **2013,** 135, 12608-12611.

(45) Ren, F.; Ding, L.; Liu, H.; Huang, Q.; Zhang, H.; Zhang, L.; Zeng, J.; Sun, Q.; Li, Z.; Gao, M., Ultra-Small Nanocluster Mediated Synthesis of $Nd^{3+}$-Doped Core-Shell Nanocrystals with Emission in the Second Near-Infrared Window for Multimodal Imaging of Tumor Vasculature. *Biomaterials* **2018,** 175, 30-43.

(46) Pan, J.; Wang, Y.; Pan, H.; Zhang, C.; Zhang, X.; Fu, Y.-Y.; Zhang, X.; Yu, C.; Sun, S.-K.; Yan, X.-P., Mimicking Drug-Substrate Interaction: A Smart Bioinspired Technology for the Fabrication of Theranostic Nanoprobes. *Adv. Funct. Mater.* **2017,** 27, 10437.

(47) Lv, R.; Yang, P.; Hu, B.; Xu, J.; Shang, W.; Tian, J., In Situ Growth Strategy to Integrate Up-Conversion Nanoparticles with Ultrasmall CuS for Photothermal Theranostics. *ACS Nano* **2017,** 11, 1064-1072.

(48) Tian, Q.; Hu, J.; Zhu, Y.; Zou, R.; Chen, Z.; Yang, S.; Li, R.; Su, Q.; Han, Y.; Liu, X., Sub-10 nm $Fe_3O_4$@$Cu_{2-x}S$ Core-Shell Nanoparticles for Dual-Modal Imaging and

Photothermal Therapy. *J. Am. Chem. Soc.* **2013,** 135, 8571-8577.

(49) Zhang, W.; Lin, W.; Pei, Q.; Hu, X.; Xie, Z.; Jing, X., Redox-Hypersensitive Organic Nanoparticles for Selective Treatment of Cancer Cells. *Chem. Mater.* **2016,** 28, 4440-4446.

(50) Zhang, W.; Lin, W.; Zheng, X.; He, S.; Xie, Z., Comparing Effects of Redox Sensitivity of Organic Nanoparticles to Photodynamic Activity. *Chem. Mater.* **2017,** 29, 1856-1863.

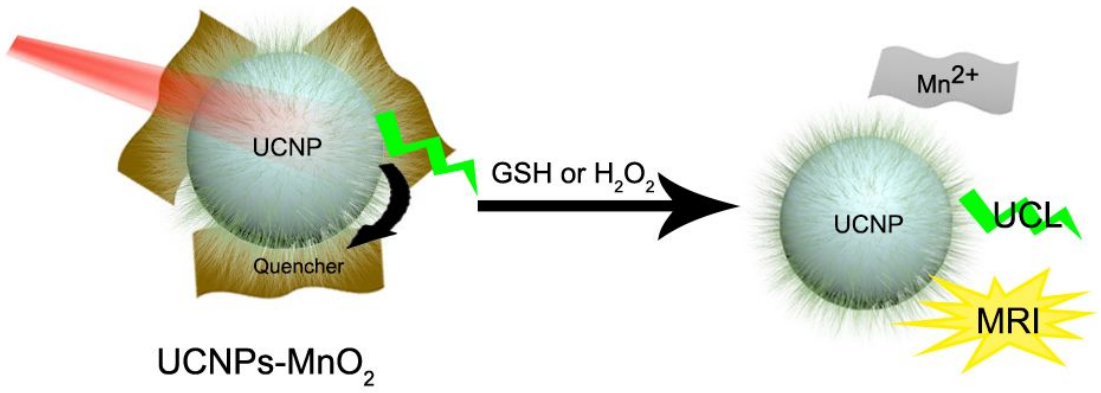


**Scheme 1** Schematic diagram of GSH/$H_2O_2$-response UCNPs-$MnO_2$.

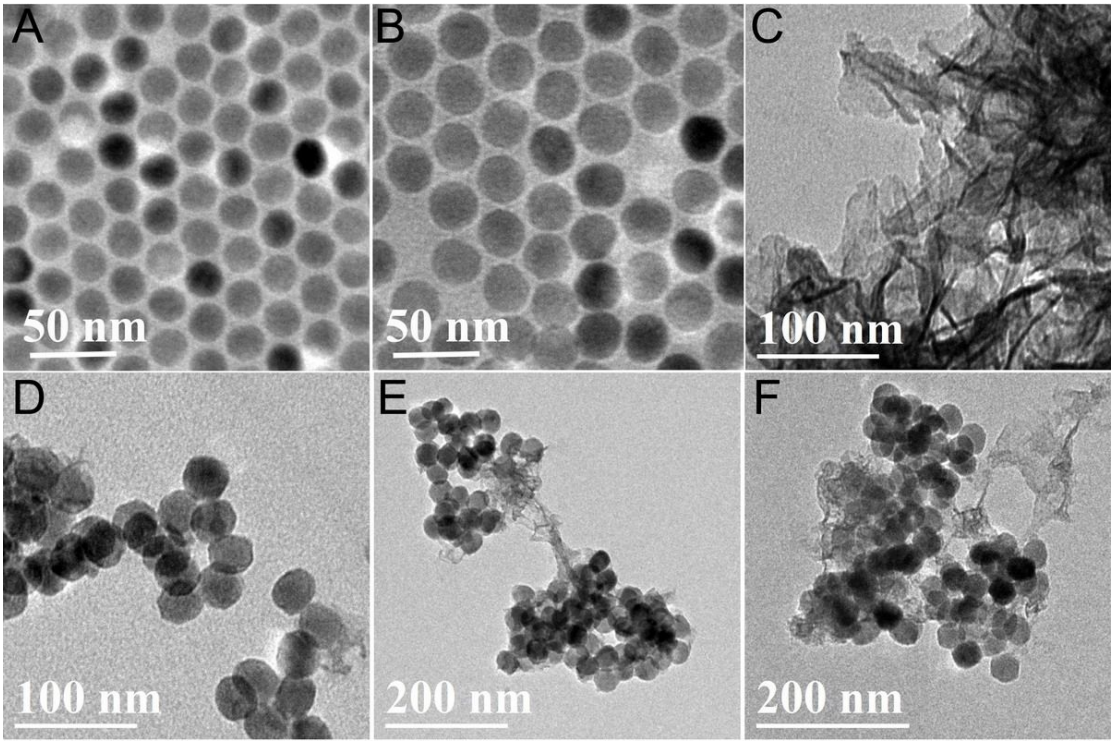


**Figure 1** TEM images of (A) core $NaYF_4$:Yb,Er, (B) core/shell $NaYF_4$:Yb,Er@$NaYF_4$:Yb,Nd (UCNPs), (C) $MnO_2$ nanosheet, and (D-F) corresponding UCNPs-$MnO_2$ as a result of increasing concentrations of $KMnO_4$ added (D) 1 mg, (E) 2 mg, (F) 3 mg.

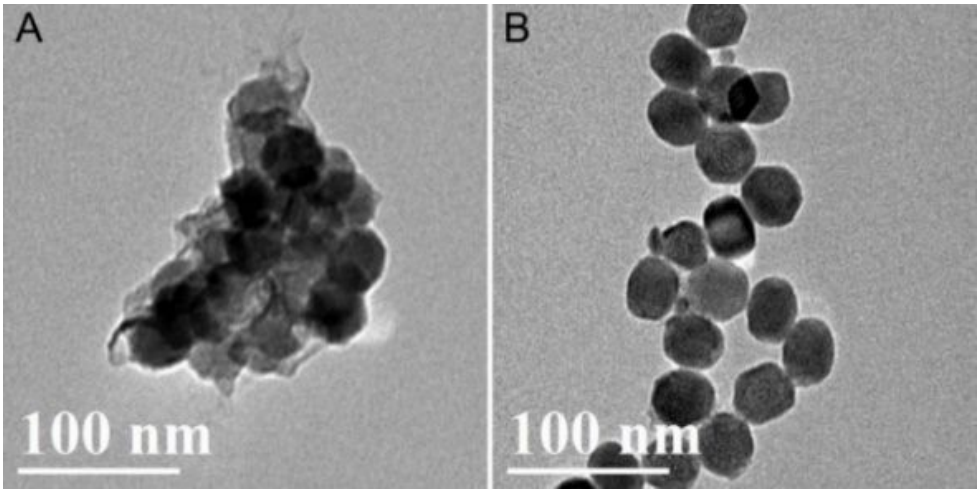


**Figure 2** TEM images of UCNPs-$MnO_2$ (A) before and (B) after addition of GSH.

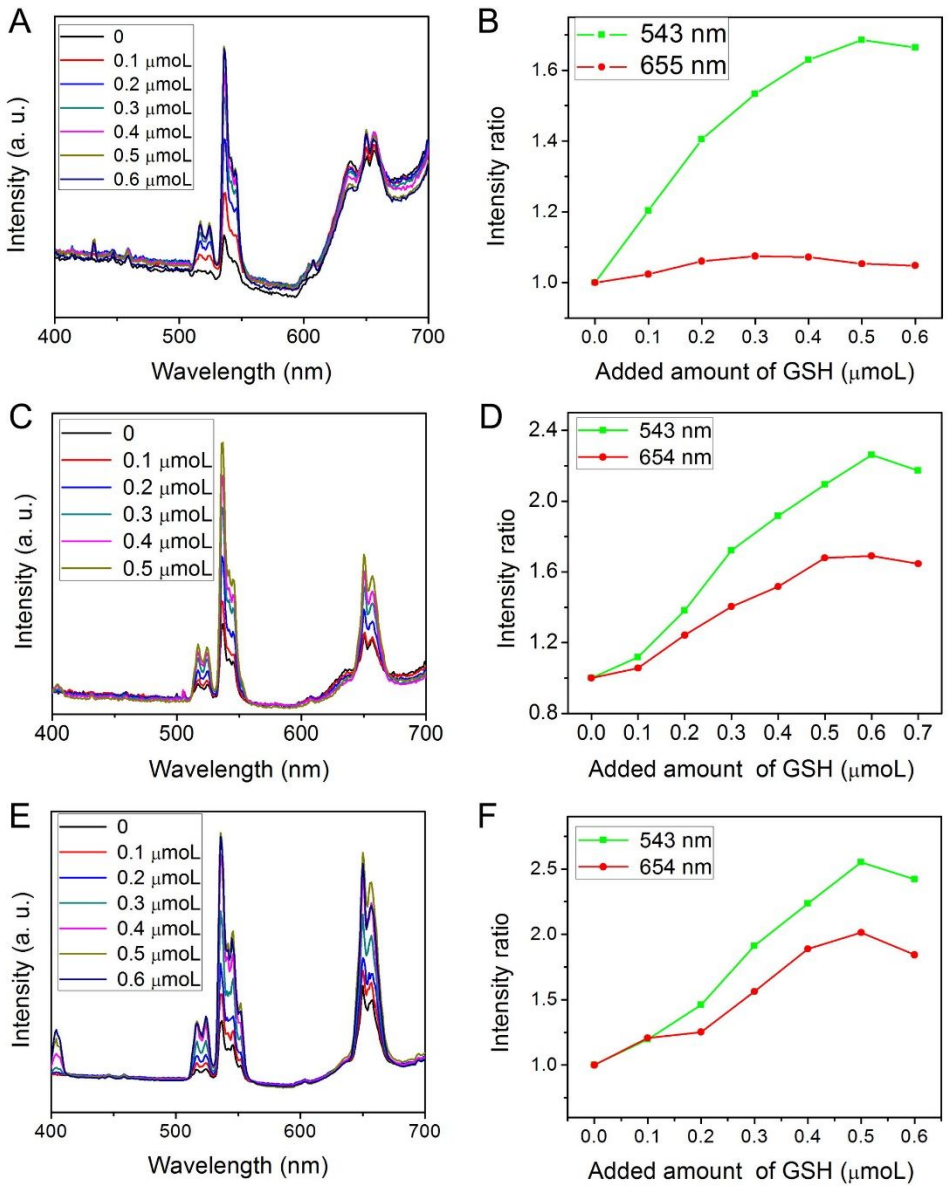


**Figure 3** (A, C, E) Spectra showing the recovery of the up-conversion luminescence of the different UCNPs-$MnO_2$ of increasing $MnO_2$ nanosheet thickness, in response to the addition of varying GSH concentrations. (B, D, F) the Corresponding enhancement factor of A, C, and E, respectively. (Excitation: 808 nm laser.)

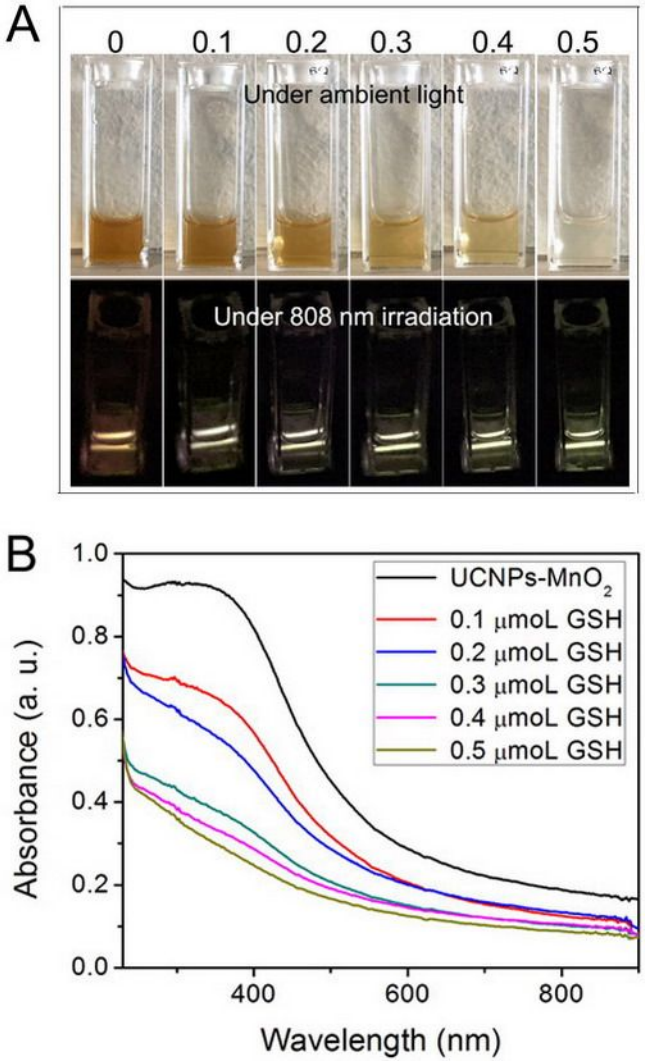


**Figure 4** (A) Photographs of the UCNPs-$MnO_2$ solutions with different concentrations of GSH added under ambient light and under 808 nm irradiation. (B) UV-vis absorption spectra curves of UCNPs-$MnO_2$ solutions with different concentrations of GSH added.

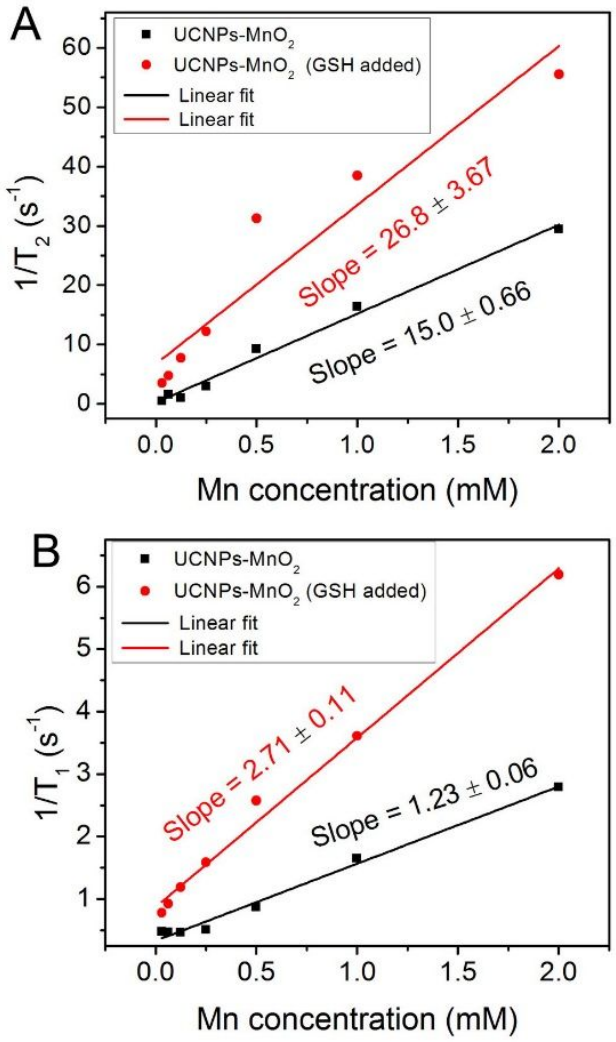


**Figure 5** (A) T2 and (B) T1 relaxation rates versus different Mn concentrations with the addition of GSH.

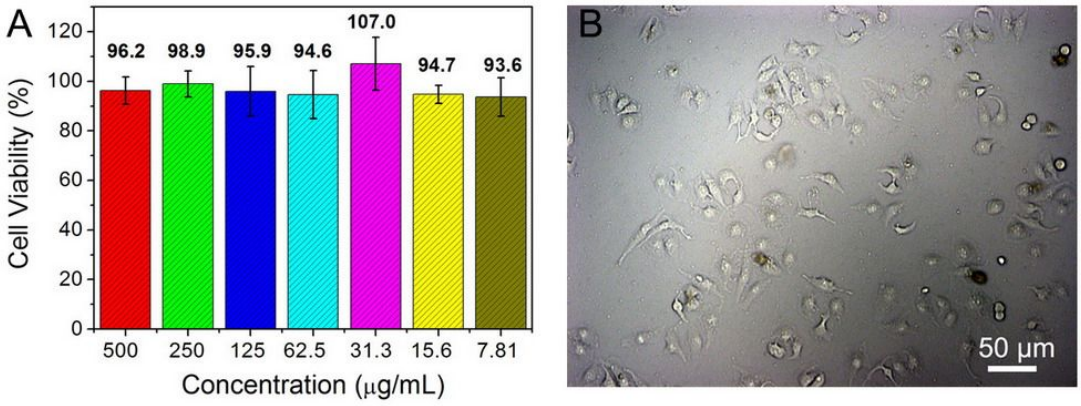


**Figure 6** (A) The viability of MCF-7 cells incubated with UCNPs-$MnO_2$ for 24 h using MTT assay. (B) The optical microscopy images of cells incubated with UCNPs-$MnO_2$.

TOC Graphic

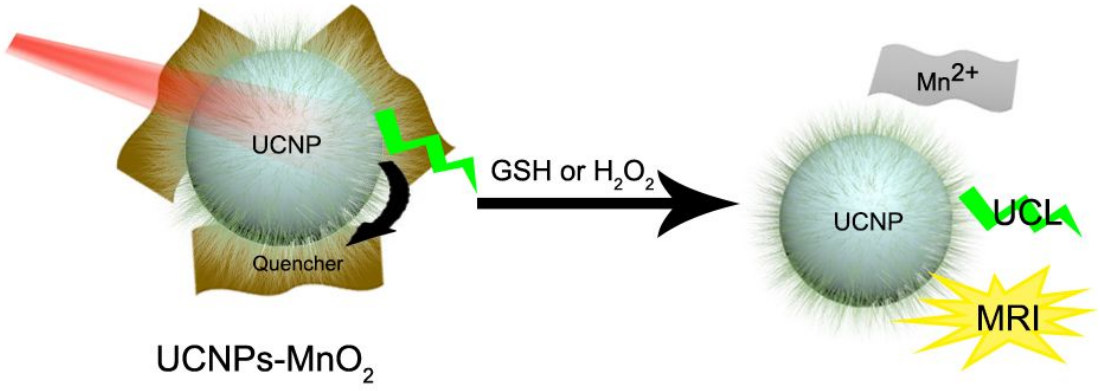


$UCNPs\text{-}MnO_2$